Journal of Computational Acoustics, Vol. 7, No. 3 (1999) 185–206

A SPACE MARCHING SCHEME FOR UNDERWATER ACOUSTIC WAVE PROPAGATION IN FLUID-ELASTIC MEDIA

TONY W. H. SHEU, S. C. CHEN, C. F. CHEN and T. P. CHIANG
Department of Naval Architecture and Ocean Engineering,
National Taiwan University, 73 Chou-Shan Rd., Taipei, Taiwan, R.O.C.

DING LEE
Department of Computer Science, Yale University,
P.O. Box 208285, New Haven, Connecticut 06520-8285, USA

Received 21 September 1998
Revised 12 February 1999

We present in this paper partial differential equations which govern three-dimensional acoustic wave propagation in fluid-elastic media. Working equations are parabolized so as to allow the analysis to be conducted in a plane-by-plane fashion. This simplification, while permitting only outgoing wave propagation, facilitates the analysis and cuts down on computing time and disk storage. To couple working equations in fluid and elastic layers, we impose physically relevant conditions on the interface. On the horizontal interface we demand continuity of the normal displacement and normal stress. In addition, physical reasoning requires that shear stresses vanish on the interface for the present analysis, which is formulated under the inviscid flow assumption. We approximate spatial derivatives with respect to θ and z using the second-order accurate centered scheme. The resulting ordinary differential equation is solved using the implicit scheme to render also second-order prediction accuracy in r. With a numerical scheme, it is highly desirable to be able to check its prediction against suitable test problems, preferably ones for which an exact solution is available. In this three-dimensional study, test problems were chosen to demonstrate the applicability of the code to the individual fluid and elastic layer. We have also verified that the code is applicable to analysis of wave propagation in water and elastic layers, across which there is an interface.

1. Introduction

Over the past few decades, intensive research efforts have been devoted to understanding ocean acoustic wave propagation. The rapid growth of high-speed computers and ever-improving numerical techniques offer distinct advantages for numerical exploration into the propagation details of acoustic waves. It is now well accepted that the computational acoustic technique has made a significant contribution to the ocean acoustics community,[1] as is evidenced by the increasing use of analysis codes developed. Most existing underwater acoustic propagation models have been developed to provide solutions to problems involving water layer. The ocean is, however, surrounded by land and is bounded above by air and

below by an elastic bottom. With this in mind, we have focused our attention on the three-dimensional elastic-fluid acoustic model. To the authors' knowledge, this work is still at an early development stage. Thus, it is necessary to provide a review of underwater acoustic wave propagation models in existence.

Early work on the subject of underwater wave propagation dates back to the work of Tappert[2] and McCoy.[3] Wales and McCoy[4] further compared different parabolic theories for modeling the elastic wave propagation in linearly elastic solids. In 1985, Greene presented a well-known model, SHAPE[5] (Seismic High-Angle PE), to permit numerical simulation of a high-angle, one-way seismic wave propagation along rough and sloping interfaces. This model was later refined by Wetton and Brooke[6] who replaced the original rational linear approximation with the bilinear square root approximation. Recently, the fluid-elastic interface problem gradually became the focal research attention aimed at gaining a better understanding of the underwater acoustic wave propagation. Early development in this area resorted to idealizations in order to make the problem tractable. Thomson and Mayfield[7] derived a local reacting boundary condition at the fluid-elastic interface to account for wave propagation in two adjacent layers. Papadakis[8] applied the "impedance + IFD" condition in their derivation of boundary condition to simulate an elastic bottom. Another important contributions to the fluid-elastic interface treatment were due to Collins[9,10] and Shang and Lee.[11] Hudson[12] was among the very few authors who considered three-dimensional elastic propagation problems. He derived working equations, written in terms of displacement variables, but made no attempt to implement them into the numerical computation. More recently, Nagem *et al.*[13] and Lee and Nagem[14] formulated a set of elastic parabolic equations, paving the way for the later derivation of a three-dimensional coupled fluid-elastic model.[15] In this paper, we develop a space-marching code for equations governing the wave propagation in fluid-elastic medium. It is hoped that this newly developed computer code provides an alternative to a simulation which has the ability to account for shear wave propagation on the fluid-elastic interface.

The outline of this paper is as follows: in Sec. 2, the parabolized differential model governing wave propagation in an ocean environment is introduced. The formulation includes sufficient details provided for the reader's reference. In order to faithfully describe the propagation details, it is important to couple two differential systems via interface conditions which dictate continuity of normal displacement and normal stresses. On the interface, it is physically rational to assume zero-shear stresses. In Sec. 3, we discretize the spatial derivatives with respect to θ and z using a second-order centered scheme. In Sec. 4, we briefly describe the space marching scheme which provides second-order accuracy in the marching direction using the implicit scheme. Owing to the use of a marching solution algorithm, it is possible to solve the three-dimensional problem plane-by-plane in a direction moving outwards from the sound source. This greatly reduces the disk storage demand and, of course, the computing time. This is followed by the fundamental study of the difference scheme. The emphasis is placed on the modified equation analysis and the stability analysis. In Sec. 6, the second-order accurate finite-difference code is validated through analytic tests to benchmark the scheme performance. Finally, Sec. 7 presents the conclusions.

2. Mathematical Model

In this section, we follow the work of Lee *et al.*[15] to rederive the mathematical model for numerical simulation of underwater acoustic wave propagation in three dimensions. As is usual in underwater wave acoustic analyses, we consider here wave propagation from a harmonic sound source. In this study, the problem is formulated in cylindrical coordinates (r, θ, z), where r, θ, and z represent the range, azimuth, and depth variables, respectively.

Given the harmonic nature of a sound source in the ocean, it is legitimate to replace the physically correct hyperbolic wave equation with the elliptic Helmholtz equation for the acoustic pressure field.[16] Following the parabolic approximation of Tappert,[2] the three-dimensional far-field equation can be reduced to a second-order homogeneous ordinary differential equation for $v(r)$ and a partial differential equation for $u(r, \theta, z)$:

$$\frac{\partial^2 v}{\partial r^2} + \frac{1}{r}\frac{\partial v}{\partial r} + k_0^2 v = 0\,, \tag{2.1}$$

$$\frac{\partial^2 u}{\partial r^2} + \left(\frac{1}{r} + \frac{2}{v}\frac{\partial v}{\partial r}\right)\frac{\partial u}{\partial r} + \frac{\partial^2 u}{\partial z^2} + \frac{1}{r^2}\frac{\partial^2 u}{\partial \theta^2} + k_0^2[n^2(r, \theta, z) - 1]u = 0\,. \tag{2.2}$$

In the above equations, $k_0(\equiv 2\pi f/c_0)$ and $n(r, \theta, z)(\equiv c_0/c(r, \theta, z))$ represent the reference wavenumber and the index of refraction, respectively. We denote that c_0 is the reference sound speed, c the sound speed, and f the source frequency. Solutions to Eq. (2.1) can be analytically represented as a combination of solutions for incoming and outgoing waves. As our attention is focused on the outgoing wave, the closed-form solution to Eq. (2.1), thus, can be represented by a zeroth-order Hankel function of the first kind $H_0^{(1)}(k_0 r)$. Upon application of the far-field approximation $(k_0 r \gg 1)$, the analytic solution $v(r)$ approaches $(2/\pi k_0 r)^{\frac{1}{2}} \exp(i(k_0 r - (\pi/4)))$.

The derivation is followed by simplifying the range variable coefficient $((1/2)+(2/v)v_r)$ as $2ik_0$. This approximation parabolizes Eq. (2.2) and, thus, facilitates the three-dimensional analysis in that solutions can be computed plane-by-plane marching outwards from the sound source. Upon application of approximation $|\partial^2 u/\partial r^2| \ll |2ik_0(\partial u/\partial r)|$ to Eq. (2.2), the parabolic equation for $u(r, \theta, z)$ can be derived as follows[1]:

$$\frac{\partial u}{\partial r} = ik_0(-1 + \sqrt{1 + X + Y})u\,, \tag{2.3}$$

where

$$X = (n^2 - 1) + \frac{1}{k_0^2}\frac{\partial^2}{\partial z^2}\,, \tag{2.4}$$

$$Y = \frac{1}{k_0^2 r^2}\frac{\partial^2}{\partial \theta^2}\,. \tag{2.5}$$

The derivation of equations is followed by considering equations which govern the propagation of harmonic waves in an inhomogeneous layer beneath the ocean. The medium of

the present interest is essentially elastic in nature. The physical properties which can represent the elastic bottom include Lame' constants, λ and μ, and density ρ. Of the potential[4] and displacement[12] approaches, we adopt the potential approach since it can be used in conjunction with the aforementioned three-dimensional scalar parabolic Eq. (2.3).

In the elastic medium, the stress tensor $\underline{\underline{\tau}}$ can be expressed as a function of the displacement vector $\underline{u}$ and Lame' constants[17]:

$$\underline{\underline{\tau}} = \lambda(\nabla \cdot \underline{u})\underline{\underline{I}} + \mu(\nabla \underline{u} + (\nabla \underline{u})^T)\,. \tag{2.6}$$

For the linear elastic medium that is locally isotropic, the propagation of time-harmonic stress wave, with a radian frequency ω, is governed by the equation

$$\nabla \cdot \underline{\underline{\tau}} + \rho\omega^2 \underline{u} = 0\,. \tag{2.7}$$

Following the Helmholtz decomposition,[13] it is appropriate to decompose the displacement vector into rotational and expansion parts. This rigorous theory permits the replacement of displacement vector $\underline{u}$ with the sum of the displacement potentials ϕ and $\underline{\psi}$ as follows[13]:

$$\underline{u} = \nabla\phi + \nabla \times \underline{\psi}\,. \tag{2.8}$$

It is noted that the vector potential $\underline{\psi}$ accommodates the divergence-free property

$$\nabla \cdot \underline{\psi} = 0\,. \tag{2.9}$$

The medium under investigation is that its Lame' constants (λ, μ) and density ρ are allowed to vary in space but are invariant in time. With this in mind, we may express the Lame' parameters, density, and displacement vector as the sum of their corresponding values, indicated by the superscript "(0)" and the much less spatially varying quantities, indicated by the superscript "(1)"; i.e. $q_i = q_i^{(0)} + q_i^{(1)}$, ($q_i = \lambda$, μ, ρ, $\underline{u}$). Substituting q_i first into Eqs. (2.8) and (2.9) and then into Eq. (2.7), a set of uncoupled Helmholtz equations can be derived in cylindrical coordinates for the leading scalar potential $\phi^{(0)}$ and the vector potential $\underline{\psi}^0 (\equiv \psi_r^{(0)}, \psi_\theta^{(0)}, \psi_z^{(0)})$.[15]

Upon substitution of $\phi = r^{\frac{-1}{2}} A(r,\ \theta,\ z) e^{ik_L r}$, $\psi_\theta = r^{\frac{-1}{2}} B_\theta(r,\ \theta,\ z) e^{ik_T r}$, $\psi_r = r^{\frac{-3}{2}} B_r(r, \theta, z) e^{ik_T r}$ and $\psi_z = r^{\frac{-1}{2}} B_z(r, \theta, z) e^{ik_T r}$ into the resulting equations, equations for unknowns A, B_z, B_r and B_θ can be derived. It is noted that ψ_r, ψ_θ, ψ_z are not linearly independent. Instead, they are constrained by the following divergence-free condition:

$$\frac{\partial \psi_r}{\partial r} + \frac{\psi_r}{r} + \frac{1}{r}\frac{\partial \psi_\theta}{\partial \theta} + \frac{\partial \psi_z}{\partial z} = 0\,. \tag{2.10}$$

To facilitate the analysis, the following two square root approximation operators are invoked in the study:

$$\sqrt{1 + X + Y} = 1 + \frac{1}{2}X - \frac{1}{8}X^2 + \frac{1}{2}Y - O(X^3, Y^2)\,, \tag{2.11}$$

$$(\sqrt{1 + X + Y})^{-1} = 1 - \frac{1}{2}X + \frac{3}{8}X^2 - \frac{1}{2}Y + O(X^3, Y^2)\,. \tag{2.12}$$

The operators shown above are defined by $X_L = (1/k_L^2)(\partial^2/\partial z^2)$, $Y_L = (1/k_L^2 r^2)(\partial^2/\partial\theta^2)$, $X_T = (1/k_T^2)(\partial^2/\partial z^2)$, $L_T = (1/k_T^2 r^2)(\partial^2/\partial\theta^2)$ where $k_L^2 = \rho\omega^2/(\lambda + 2\mu)$, $k_T^2 = \rho\omega^2/\mu$. Substitution of Eqs. (2.11) and (2.12) into equations for A, B_z, B_r and B_θ yields

$$\frac{\partial A}{\partial r} = ik_L \left(\frac{1}{2}X_L - \frac{1}{8}X_L^2 + \frac{1}{2}Y_L\right) A\,, \tag{2.13}$$

$$\frac{\partial B_z}{\partial r} = ik_T \left(\frac{1}{2}X_T - \frac{1}{8}X_T^2 + \frac{1}{2}Y_T\right) B_z\,, \tag{2.14}$$

$$\frac{\partial B_r}{\partial r} = ik_T \left(\frac{1}{2}X_T - \frac{1}{8}X_T^2 + \frac{1}{2}Y_T\right) B_r - \frac{1}{2ik_T}\left(1 - \frac{1}{2}X_T + \frac{3}{8}X_T^2 - \frac{1}{2}Y_T\right)\frac{\partial B_z}{\partial z}\,, \tag{2.15}$$

$$\frac{\partial B_\theta}{\partial r} = ik_T \left(\frac{1}{2}X_T - \frac{1}{8}X_T^2 + \frac{1}{2}Y_T\right) B_\theta - \frac{1}{2ik_T}\left(1 - \frac{1}{2}X_T + \frac{3}{8}X_T^2 - \tfrac{1}{2}Y_T\right)\frac{2}{r^3}\frac{\partial B_r}{\partial\theta}\,. \tag{2.16}$$

3. Interface Conditions

The formulation remains to prescribe conditions on the interface between the elastic medium and the fluid layer and results in a well-posed problem. For simplicity, the fluid-elastic interface is assumed to be a plane. Field variables at the horizontal interface can be calculated either from the layer above the interface or from the layer below it. We use the subscript "1" to indicate the fluid layer and the subscript "2" to denote the elastic medium. On physical grounds, displacement vectors are continuous across the interface of two media. Thus, continuity of normal displacement implies that

$$\frac{\partial\phi_1}{\partial z} = \frac{\partial\phi_2}{\partial z} + \frac{\psi_\theta}{r} + \frac{\partial\psi_\theta}{\partial r} - \frac{1}{r}\frac{\partial\psi_r}{\partial\theta}\,. \tag{3.1}$$

Another interface condition is derived by considering normal stress components. Physical reasoning dictates continuity of normal stresses between layers of different media:

$$-\rho\omega^2\phi_1 = -\lambda k_L^2\phi_2 + 2\mu\left(\frac{\partial^2\phi_2}{\partial z^2} + \frac{\partial^2\psi_\theta}{\partial r\partial z} + \frac{1}{r}\frac{\partial\psi_\theta}{\partial z} - \frac{1}{r}\frac{\partial^2\psi_r}{\partial\theta\partial z}\right)\,. \tag{3.2}$$

Given that the liquid above the interface is inviscid, two shear components tangential to the horizontal interface must vanish. This gives the following interface conditions needed to blend two adjacent layers having different material properties:

$$\frac{2}{r}\frac{\partial^2\phi_2}{\partial\theta\partial z} + \frac{1}{r}\frac{\partial^2\psi_\theta}{\partial r\partial\theta} + \frac{1}{r^2}\frac{\partial\psi_\theta}{\partial\theta} - \frac{1}{r^2}\frac{\partial^2\psi_r}{\partial\theta^2} + \frac{\partial^2\psi_r}{\partial z^2} - \frac{\partial^2\psi_z}{\partial r\partial z} = 0\,, \tag{3.3}$$

$$2\frac{\partial^2\phi_2}{\partial r\partial z} + \frac{\partial^2\psi_\theta}{\partial r^2} + \frac{1}{r}\frac{\partial\psi_\theta}{\partial r} - \frac{\psi_\theta}{r^2} - \frac{\partial^2\psi_\theta}{\partial z^2} + \frac{1}{r^2}\frac{\partial\psi_r}{\partial\theta} + \frac{1}{r}\frac{\partial^2\psi_z}{\partial z\partial\theta} - \frac{1}{r}\frac{\partial^2\psi_r}{\partial r\partial\theta} = 0\,. \tag{3.4}$$

To make the mathematical model well posed for the simulation of acoustic wave propagation in the fluid-elastic environment, it is also important to demand satisfaction of the divergence-free equation, given in (2.10), on the interface.

For the sake of coupling equations defined in their respective layers, the interface conditions derived above are reformulated according to the factorization described earlier for the medium in the elastic layer. The resulting interface conditions, indicated by the superscript "I", are as follows:

$$\frac{1}{r}\frac{\partial B_r^I}{\partial r} + \frac{1}{r} ik_T B_r^I + \frac{1}{r}\frac{\partial B_\theta^I}{\partial \theta} + \frac{\partial B_z^I}{\partial z} = 0\,, \tag{3.5}$$

$$\frac{\partial u^I}{\partial z} e^{ik_0 r} = \frac{\partial A^I}{\partial z} e^{ik_L r} + \left(\frac{\partial B_\theta^I}{\partial r} + B_\theta^I ik_T - \frac{1}{r^2}\frac{\partial B_r^I}{\partial \theta} \right) e^{ik_T r}\,, \tag{3.6}$$

$$\begin{aligned} -\rho\omega^2 u^I e^{ik_0 r} = & \left(-\lambda k_L^2 A^I + 2\mu \frac{\partial^2 A^I}{\partial z^2} \right) e^{ik_L r} \\ & + 2\mu \left[\frac{\partial^2 B_\theta^I}{\partial r \partial z} + ik_T \frac{\partial B_\theta^I}{\partial z} - \frac{1}{r^2}\frac{\partial^2 B_r^I}{\partial \theta \partial z} \right] e^{ik_T r}\,, \end{aligned} \tag{3.7}$$

$$\begin{aligned} 0 = & \frac{2}{r}\frac{\partial^2 A^I}{\partial \theta \partial z} e^{ik_L r} + \Big(-\frac{1}{r^3}\frac{\partial^2 B_r^I}{\partial \theta^2} + \frac{1}{r}\frac{\partial^2 B_r^I}{\partial z^2} + \frac{1}{r}\frac{\partial^2 B_\theta^I}{\partial r \partial \theta} \\ & + \frac{1}{r} ik_T \frac{\partial B_\theta^I}{\partial \theta} - \frac{\partial^2 B_z^I}{\partial r \partial z} - ik_T \frac{\partial B_z^I}{\partial z} \Big) e^{ik_T r}\,, \end{aligned} \tag{3.8}$$

$$0 = \left(2\frac{\partial^2 A^I}{\partial r \partial z} + 2ik_L \frac{\partial A^I}{\partial z} \right) e^{ik_L r} + \left(-2\frac{\partial^2 B_\theta^I}{\partial z^2} - k_T^2 B_\theta^I + \frac{2}{r}\frac{\partial^2 B_z^I}{\partial \theta \partial z} \right) e^{ik_T r}\,. \tag{3.9}$$

Following the same idea of finite difference approximation of spatial derivatives with respect to z and θ, as considered in Ref. 15, the resulting matrix equation for field variables on the interface is

$$\frac{\partial}{\partial r}(A^I,\, B_z^I,\, B_r^I,\, B_\theta^I)^T = [d_{ij}](A^I,\, B_z^I,\, B_r^I,\, B_\theta^I)^T + S \tag{3.10}$$

where

$$[d_{ij}] = \begin{bmatrix} \Delta z i k_L \frac{\partial}{\partial z} & \frac{\Delta z}{r} e^{i(k_T - k_L)r} \frac{\partial^2}{\partial \theta \partial z} & 0 & -\Delta z e^{i(k_T - k_L)r} \left(\frac{\partial^2}{\partial z^2} + \frac{k_T^2}{2} \right) \\ -\frac{2}{r}\Delta z e^{i(k_L - k_T)r} \frac{\partial^2}{\partial \theta \partial z} & ik_T \Delta z \frac{\partial}{\partial z} & \Delta z \left(\frac{1}{r^3}\frac{\partial^2}{\partial \theta^2} - \frac{1}{r}\frac{\partial^2}{\partial z^2} \right) & -\Delta z \frac{ik_T}{r}\frac{\partial}{\partial \theta} \\ 0 & -r\frac{\partial}{\partial z} & -ik_T & -\frac{\partial}{\partial \theta} \\ -\Delta z e^{i(k_L - k_T)r} \left(\frac{\lambda}{2\mu} k_L^2 \frac{\partial^2}{\partial z^2} \right) & 0 & \frac{-\Delta z}{r^2}\frac{\partial^2}{\partial \theta \partial z} & \Delta z i k_T \frac{\partial}{\partial z} \end{bmatrix} \tag{3.11}$$

and

$$[S] = \begin{bmatrix} \left(\dfrac{\partial A}{\partial r}\right)_{M+1,l} \\ \left(\dfrac{\partial B_z}{\partial r}\right)_{M+1,l} - \dfrac{\Delta z}{r}\dfrac{1}{2\Delta\theta}\left[\left(\dfrac{\partial B_\theta^I}{\partial r}\right)_{M,l+1} - \left(\dfrac{\partial B_\theta^I}{\partial r}\right)_{M,l-1}\right] \\ 0 \\ \gamma\Delta z e^{i(k_0-k_T)r} u_{M-1,l} + \left(\dfrac{\partial B_\theta}{\partial r}\right)_{M+1,l} \end{bmatrix}. \tag{3.12}$$

Interested readers should refer to Ref. 18 for additional details of the derivation of equations given in (3.10–3.12).

Before proceeding to the numerical analysis of fluid-elastic acoustic wave propagation equations which are coupled through interface conditions, it is instructive to summarize here the differential system as follows:

$$\frac{\partial \underline{U}}{\partial r} = \underline{\underline{M}}\,\underline{U} + \underline{N} \tag{3.13}$$

where $\underline{U}$ represents the solution vector $\underline{U} = (u, A^I, B_z^I, B_r^I, B_\theta^I, A, B_z, B_r, B_\theta)^T$. In the above equation, $\underline{N}$ is the vector function resulting solely from the interface condition. The coefficients in the matrix equation $M_{ij}(i = 1 \sim 9)$ are detailed in Ref. 18.

4. Space Marching Solution Algorithm

The first step in solving the matrix equation (3.13) is to discretize spatial derivatives with respect to z and θ. The inherent physical nature of these terms allows us to discretize them using the centered scheme to render second-order accuracy in θ and z. Having discretized equations with respect to θ and z, the finite difference solutions can then be solved from the resulting ordinary differential equation.

The solutions to Eq. (3.13) are solved in a plane-by-plane fashion, starting from the initial solution plane $r = r_0$. The analysis is followed by forward marching in the direction of an increasing value of r. Within each marching step Δr, the solutions at the solution plane are computed from

$$\underline{U}^{n+1} - \underline{U}^{(n+1)/2} = \frac{\Delta r}{2}\underline{\underline{M}}^{(n+1)/2}\underline{U}^{(n+1)/2} + \frac{\Delta r}{2}\underline{N}^{(n+1)/2}, \tag{4.1}$$

or

$$\underline{U}^{n+1} = \left(1 + \frac{\Delta r}{2}\underline{\underline{M}}^{(n+1)/2}\right)\underline{U}^{(n+1)/2} + \frac{\Delta r}{2}\underline{N}^{n+1/2}. \tag{4.2}$$

Upon substitution of $\underline{\underline{M}}^{n+1/2} = (1/2)(\underline{\underline{M}}^{n+1} + \underline{\underline{N}}^{n})$, $\underline{U}^{n+1/2} = (1/2)(\underline{U}^{n+1} + \underline{U}^{n})$ and $\underline{N}^{n+1/2} = (1/2)(\underline{N}^{n+1} + \underline{N}^{n})$ into Eq. (4.1), the following equation is derived to compute the solution vector $\underline{U}^{n+1}$:

$$\underline{U}^{n+1} = \left[1 - \frac{\Delta r}{4}(\underline{\underline{M}}^{n+1} + \underline{\underline{M}}^{n})\right]^{-1} \left\{\left[1 + \frac{\Delta r}{4}(\underline{\underline{M}}^{n+1} + \underline{\underline{M}}^{n})\right]\underline{U}^{n} + \frac{\Delta r}{2}(\underline{N}^{n} + \underline{N}^{n+1})\right\} . \tag{4.3}$$

Iteration continues to update the matrix $\underline{\underline{M}}$ and vector $\underline{N}$ until the tolerance specified *a priori* for convergence of $\underline{U}^{n+1}$ is reached. The above marching solution algorithm is shown in Sec. 5 to provide second-order accuracy in r. Thus, the discretization scheme chosen here provides uniform second-order accuracy in all spatial directions.

To obtain a better understanding of the matrix equation from which $\underline{U}$ is solved, we plot in Fig. 1 the profile of the coefficient matrix. As seen in the figure this matrix is characterized by sparsity and asymmetry. This matrix also shows a rich and complex interaction structure between the fluid and elastic media. Clearly evident in Fig. 1 is the interface conditions which largely increase the matrix sparseness and, thus, complicate the analysis.

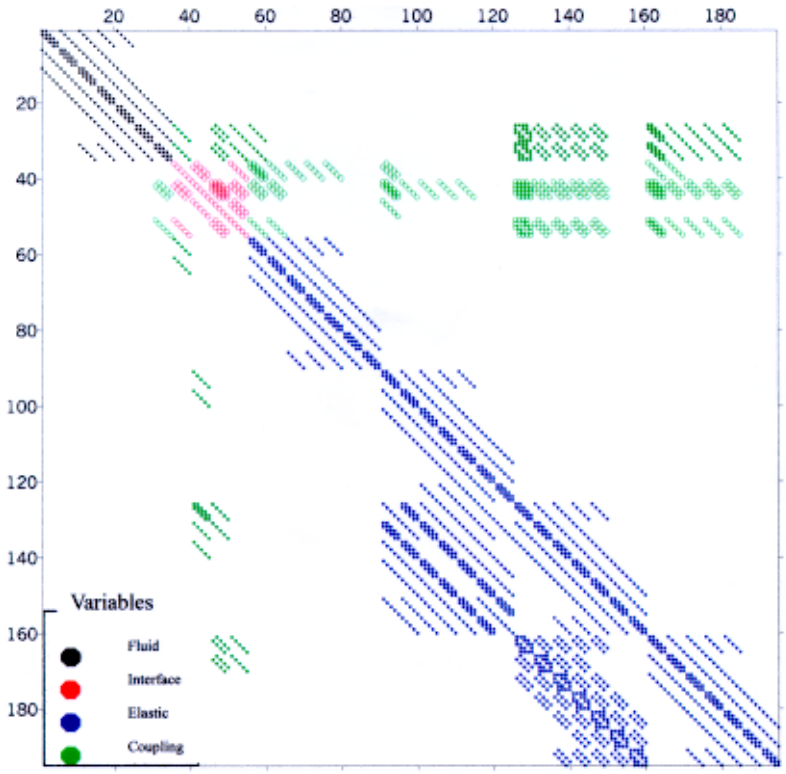

Fig. 1. The matrix profile obtained from fluid-elastic differential equations at a fixed radial plane r. The number in the figure represents the row and column of the 200×200 matrix equation.

5. Fundamental Study of the Discretization Scheme

Efforts to obtain a full understanding of the finite difference scheme applied to simulate wave equations in fluid and elastic layers require detailed knowledge of the scheme feature. As is common in fundamental study of the finite difference scheme, we conduct in fluid and elastic media modified equation analyses of the discretized equations, from which the accuracy order of the scheme can be obtained. Von-Neumann stability analysis is also conducted to make sure that stable solutions can be obtained.

For the purpose of conducting fundamental study of the working equation in the fluid layer, we write the working equation for u as follows:

$$\frac{\partial u}{\partial r} = au + bu_{zz} + cu_{zzzz} + du_{\theta\theta}\,, \tag{5.1}$$

where

$$a = \frac{ik_0}{2}(n^2-1) - \frac{ik_0}{8}(n^2-1)^2\,, \tag{5.2}$$

$$b = \frac{i}{2k_0} - \frac{i(n^2-1)}{4k_0}\,, \tag{5.3}$$

$$c = \frac{-i}{8k_0^3}\,, \tag{5.4}$$

$$d = \frac{i}{2k_0 r^2}\,. \tag{5.5}$$

To assure the stability of the discretization scheme used in this study, we perform Taylor series expansion of the terms shown in the finite-difference equation of (5.1) to yield

$$u_{m,l}^{n+1} = \left(1 + a\Delta r - 2\Delta r\frac{b}{\Delta z^2} + 6\Delta r\frac{c}{\Delta z^4} - 2\Delta r\frac{d}{\Delta\theta^2}\right) u_{m,l}^n + \Delta r\frac{b}{\Delta z^2}(u_{m+1,l}^n + u_{m-1,l}^n)$$
$$+ \Delta r\frac{c}{\Delta z^4}(u_{m+2,l}^n - 4u_{m+1,l}^n - 4u_{m-1,l}^n + u_{m-2,l}^n) + \Delta r\frac{d}{\Delta\theta}(u_{m,l+1}^n + u_{m,l-1}^n)\,. \tag{5.6}$$

We then approximate $u_{m\pm f,l\pm g}^{n+k} = \xi^{n+k} e^{iP\Delta z(m\pm f)} e^{iQ\Delta\theta(l\pm g)}$ $(k = 0,\ 1;\ f = 1,\ 2;\ g = 1)$ and substitute them into Eq. (5.6). After tedious mathematical effort, we can derive the amplification factor as follows:

$$\xi \equiv \frac{u_{m,l}^{n+1}}{u_{m,l}^n} = \frac{1 - iA}{1 + iA}\,, \tag{5.7}$$

where A involves the wavenumber in the z-direction, P, and the wavenumber in the

θ-direction, Q:

$$A = \frac{1}{2}\Delta r\left[\frac{k_0}{2}(n^2-1) - \frac{k_0}{8}(n^2-1)^2\right] + \frac{\Delta r}{\Delta z^2}\left[\frac{1}{2k_0} - \frac{(n^2-1)}{4k_0}\right][1-\cos(P\Delta z)]$$
$$+ \frac{\Delta r}{\Delta z^4}\frac{1}{8k_0^3}[3+\cos(2P\Delta z) - 4\,\cos(P\Delta z)] + \frac{\Delta r}{\Delta\theta^2}\frac{1}{2k_0 r^2}[1-\cos(Q\Delta\theta)]\,. \qquad (5.8)$$

The essential feature of the amplification factor shown in Eq. (5.7) is that its magnitude is unconditionally less than one. Thus, the discretization method employed here is considered to be able to provide stable solutions.

The analysis is followed by deriving the modified equation for Eq. (5.1). By conducting Taylor series expansions on every term shown in (5.6), we can derive the modified equation:

$$\frac{\partial u}{\partial r} - au - bu_{zz} - cu_{zzzz} - du_{\theta\theta}$$
$$= \left\{\Delta r\left(\frac{\partial u}{\partial r}\right) - (a\Delta r)u^n_{m,l} - b\Delta r\left(\frac{\partial^2 u}{\partial z^2}\right) - c\Delta r\left(\frac{\partial^4 u}{\partial z^4}\right) - d\Delta r\left(\frac{\partial^2 u}{\partial\theta^2}\right)\right\}$$
$$+\left[\frac{\Delta r^2}{2!}\left(\frac{\partial^2 u}{\partial r^2}\right) + \frac{\Delta r^3}{3!}\left(\frac{\partial^3 u}{\partial r^3}\right) + \frac{\Delta r^4}{4!}\left(\frac{\partial^4 u}{\partial r^4}\right)\right.$$
$$\left. - b\Delta r\frac{(\Delta z)^2}{12}\left(\frac{\partial^4 u}{\partial z^4}\right) - d\Delta r\frac{(\Delta\theta)^2}{12}\left(\frac{\partial^4 u}{\partial\theta^4}\right)\right]. \qquad (5.9)$$

This modified equation justifies the scheme accuracy. The scheme is clearly shown to have the potential of producing an accuracy order of $O(\Delta r^2, \Delta r\Delta z^2, \Delta r\Delta\theta^2)$, thereby revealing that the present discretization scheme accommodates the consistency property. Based on the above two fundamental studies, which assure scheme stability and consistency, the resulting scheme can be used with confidence to obtain convergent acoustic solutions in the water layer. The underlying theory to draw the above conclusion is based on the equivalent theorem of Lax.[20,21]

Given that some insight into the details of the scheme can be obtained through the stability and modified equation analyses, the same fundamental study was undertaken on elastic equations in order to provide justification for the validity of the three-dimensional elastic finite-difference model. An examination of differential equations applied to elastic media reveals that each equation bears a close resemblance to the equation in the water. They differ only in the physical meaning of the field variable u and, of course, the expressions a, b, c, d shown in (5.1). Using the approach similar to that considered earlier, the amplification factor for the scheme applied to the elastic layer is obtained as

$$|\xi| = \left|\frac{1 - iA_{\text{elastic}}}{1 + iA_{\text{elastic}}}\right|, \qquad (5.10)$$

where

$$A = \frac{1}{2k_0}\frac{\Delta r}{\Delta z^2}[1-\cos(P\Delta z)] + \frac{\Delta r}{\Delta z^4}\frac{1}{8k_0^3}[3+\cos(2P\Delta z)-4\cos(P\Delta z)]$$
$$+ \frac{\Delta r}{\Delta\theta^2}\frac{1}{2k_0 r^2}[1-\cos(Q\Delta\theta)]\,. \tag{5.11}$$

To this point we can conclude from Eq. (5.10) that the proposed scheme is also unconditionally stable.

To obtain accuracy order of the scheme employed in this study, we also conduct modified equation analysis for a representative equation in the elastic medium. While the derivation of the modified equation is elaborate, it is worthwhile since this theoretical analysis, which predicts an accuracy order $O(\Delta r^2, \Delta r\Delta z^2, \Delta r\Delta\theta^2)$ enables us to know that the scheme accommodates the consistency property for equations governing the acoustic wave propagation in elastic media. By Lax's equivalent theorem,[20,21] convergent solutions can be obtained without a doubt.

6. Numerical Results

Before any computational results can be deemed reliable enough to help us understand better the physical phenomena, the computational model must be validated analytically. Exact solutions to the present investigated working equations are possible in only a few select cases with very special geometry and boundary condition. These solutions, when they exist, are essential for the validation of numerical models proposed and computer codes developed. In this study, we considered three analytic problems which are chosen to demonstrate the applicability of the code to simulation of acoustic wave propagation in a water layer, in an elastic layer, and, of course, in a water-elastic layer.

6.1. *Analytic validation study in the water layer*

The first problem was chosen to verify the code, which is only applicable to a water layer. This problem was first tested by Ewing *et al.*[22] to demonstrate the validity of their derivation. As a demonstration problem, we modified our three-dimensional code by reducing one dimension so that the computed solutions could be compared with the exact solutions u_{exact} given originally in Ref. 11.

$$u_{\text{exact}} = \frac{2\pi}{H}\sqrt{\frac{2}{\pi r}}\sum_n \frac{1}{\sqrt{k_n}} e^{i(\omega t - k_n r - \frac{\pi}{4})}\Phi_1(k_n)\sin(\xi_n d)\sin(\xi_n z)\,, \tag{6.1}$$

where

$$\Phi_1(k_n) = \frac{-\left(\frac{\rho_1}{\rho_2}\right)\left(\frac{c^4}{\beta_2^4}\right)\left(\frac{\eta_n}{\xi_n}\right)k_n H}{\sqrt{\frac{c_2}{v_1^2} - IQ_n}\cos(\xi_n H)}\,, \tag{6.2}$$

$$Q_n = \frac{\rho_1}{\rho_2}\frac{c^4}{\beta_2^4}\left[\frac{\sin(\xi_n H)}{\sqrt{\frac{c^2}{v_1^2}-1}\sqrt{1-\frac{c^2}{\alpha_2^2}}}\left(1+\frac{1-\frac{c^2}{\alpha_2^2}}{\frac{c^2}{v_1^2}-1}\right)-\left(\frac{k_n H\sqrt{1-\frac{c^2}{\alpha_2^2}}}{\sqrt{\frac{c^2}{v_1^2}-1}}\sec(\xi_n H)\right)\right]$$

$$-4\left[\frac{\sqrt{1-\frac{c^2}{\beta_2^2}}}{\sqrt{1-\frac{c^2}{\alpha_2^2}}}+\frac{\sqrt{1-\frac{c^2}{\alpha_2^2}}}{\sqrt{1-\frac{c^2}{\beta_2^2}}}+2\sqrt{1-\frac{c^2}{\alpha_2^2}}\sqrt{1-\frac{c^2}{\beta_2^2}}-2\left(2-\frac{c^2}{\beta_2^2}\right)\right]\cos(\xi_n H)\,, \quad (6.3)$$

$$\xi_n = k_n\sqrt{\frac{c^2}{v_1^2}-1}\,, \quad (6.4)$$

$$\eta_n = k_n\sqrt{1-\frac{c^2}{\alpha_2^2}}\,, \quad (6.5)$$

$$k_n = 2\pi\frac{f}{c}\,. \quad (6.6)$$

In this study, material properties and flow conditions were chosen to be the same as those given in Ref. 11. These values are $H = 100$ cm, $\rho_1 = 1$ g/cm^3, $\rho_2 = 1.97$ g/cm^3, $c_1 = 1507.5$ m/s, $\alpha_2 = 1725$ m/s, $v_1 = 1500$ m/s, $f = 68.03$ Hz, $d = 25$ m, $\beta_2 = 1530$ m/s. For additional details of this test problem, the reader is referred to the work of Shang and Lee.[11]

In the rectangular physical domain, 1000 m $\leq r \leq$ 1020 m, $0 \leq z \leq 1000$ m all the calculations were performed on uniform grids of different grid resolutions. The prediction errors computed on continuously refined grids are cast in the $L_2 - norm$. As shown in Table 1, which tabulates the $L_2 - error$ norms, we can computationally demonstrate the validity of the code applied to the water layer. For completeness, we also compare the computed and exact solutions at some selected (θ, z) locations. As is evident from Fig. 2, which plots the ratios of two sets of data against r, the computed solutions compare favorably with the corresponding exact solutions.

6.2. *Analytic validation study in the elastic layer*

To verify the applicability of the code to simulation of equations in the elastic bottom, we considered the wave propagation in an unbounded three-dimensional elastic layer. The problem chosen was first studied by Rayleigh[23] and later considered by Lee *et al.*[24] This test problem is characterized by having the following exact solutions:

$$A_{\text{exact}} = -\frac{F_0}{4\pi\rho\omega^2}\frac{ik_L r^{3/2}\cos\theta\, e^{ik_L(\sqrt{r^2+z^2}-r)}}{r^2+z^2}\,, \quad (6.7)$$

$$(B_r)_{\text{exact}} = \frac{F_0}{4\pi\rho\omega^2}\frac{ik_T z r^{3/2}\sin\theta\, e^{ik_T(\sqrt{r^2+z^2}-r)}}{r^2+z^2}\,, \tag{6.8}$$

$$(B_\theta)_{\text{exact}} = \frac{F_0}{4\pi\rho\omega^2}\frac{ik_T z r^{1/2}\cos\theta\, e^{ik_T(\sqrt{r^2+z^2}-r)}}{r^2+z^2}\,, \tag{6.9}$$

$$(B_z)_{\text{exact}} = \frac{F_0}{4\pi\rho\omega^2}\frac{ik_T r^{3/2}\sin\theta\, e^{ik_T(\sqrt{r^2+z^2}-r)}}{r^2+z^2}\,, \tag{6.10}$$

where $K_L = (\rho\omega^2/(\lambda+2\mu))^{1/2}$, $K_T = (\rho\omega^2/\mu)^{1/2}$, $F_0 = \rho\iiint Q d\Omega$. It is noted that Q is a concentrated (or delta function) force per unit mass placed at the origin. In this study, we start the computation at the range value $r = 200$ m and terminate the analysis at the range value $r = 210$ m using a range increment $\Delta r = 1$ m. All physical parameters needed to compute the numerical solutions in physical domain bounded by 200 m $\leq r \leq$ 210 m, $-\Delta\theta \leq \theta \leq \Delta\theta$, and $0 \leq z \leq 5\Delta z$ are chosen the same as those given in Ref. 23. These values are $\rho = 2400$ kg/m^3, $\omega = 1000\ \pi$Hz and $\Delta\theta = 1^\circ$.

Table 1. The computed L_2–*error* norms for the test problem, given in Sec. 6.1, at different marching locations. The solutions are computed on uniform grids of different sizes, $\Delta = 5$ m, 6.25 m, 10 m.

r	$\Delta = 10$ m	$\Delta = 6.25$ m	$\Delta = 5$ m
1001	3.751150E−05	3.689550E−05	3.678120E−05
1002	7.499360E−05	7.388670E−05	7.365480E−05
1003	1.125600E−04	1.109720E−04	1.106200E−04
1004	1.501100E−04	1.481250E−04	1.476670E−04
1005	1.877480E−04	1.854140E−04	1.847770E−04
1006	2.255690E−04	2.227970E−04	2.220380E−04
1007	2.634610E−04	2.602190E−04	2.593790E−04
1008	3.014000E−04	2.977660E−04	2.968080E−04
1009	3.394720E−04	3.353980E−04	3.343700E−04
1010	3.776580E−04	3.731360E−04	3.720470E−04
1011	4.161540E−04	4.109790E−04	4.098420E−04
1012	4.551400E−04	4.488950E−04	4.477790E−04
1013	4.947700E−04	4.869240E−04	4.858110E−04
1014	5.352890E−04	5.250920E−04	5.239420E−04
1015	5.768340E−04	5.633850E−04	5.621530E−04
1016	6.195150E−04	6.017890E−04	6.003780E−04
1017	6.633880E−04	6.402870E−04	6.386780E−04
1018	7.084520E−04	6.789010E−04	6.768970E−04
1019	7.547600E−04	7.176100E−04	7.149860E−04

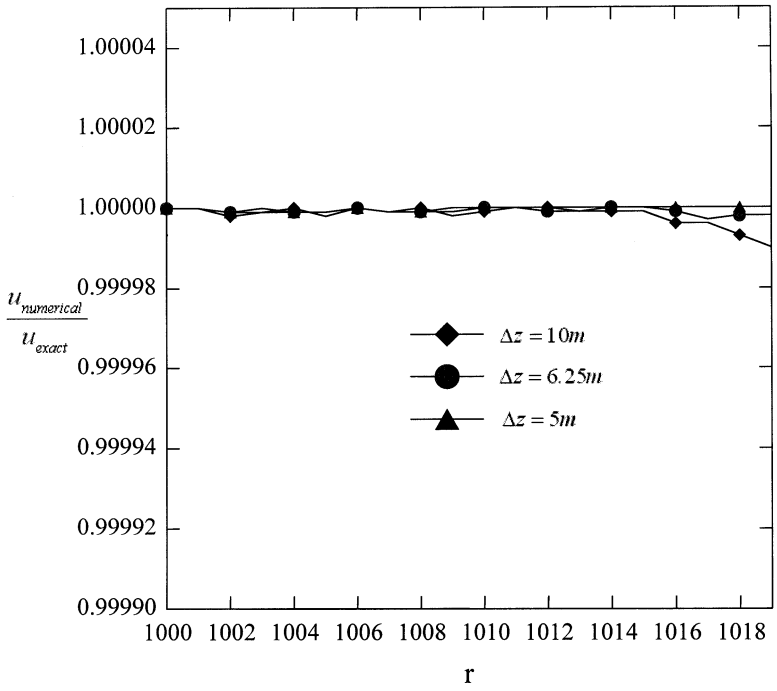

Fig. 2. The computed ratios between the numerical and exact solutions against r for the problem considered in Sec. 6.1.

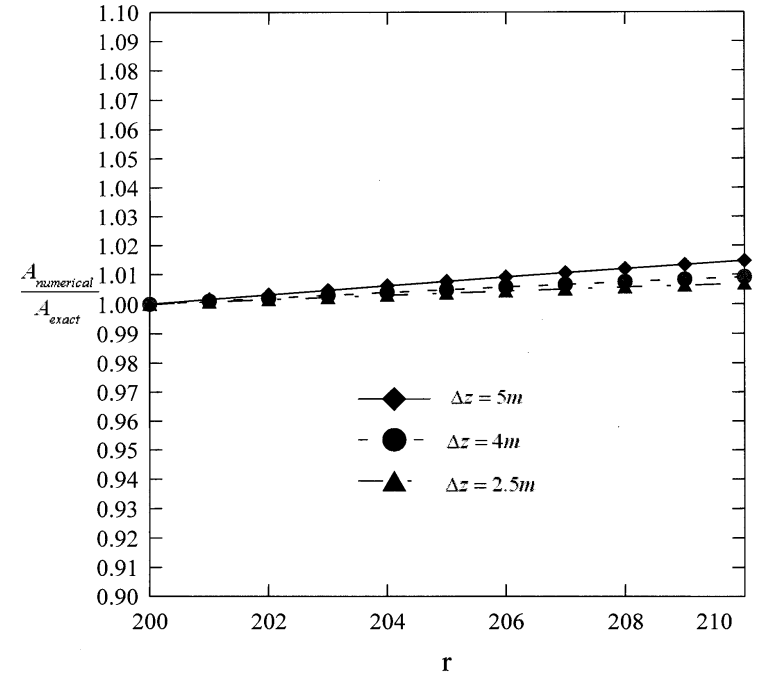

Fig. 3. The computed ratios between the numerical and exact solutions for the field variable A against r for the problem considered in Sec. 6.2.

As shown in Figs. 3–6, our finite-difference solutions for dependent variables compare well with the analytic solutions. With the code thus validated, we further assessed the marching scheme through a rate of convergence test. The predicted L_2–*error* norms computed on continuously refined grids are tabulated in Table 2, from which the rate of convergence can be obtained, as seen in the table.

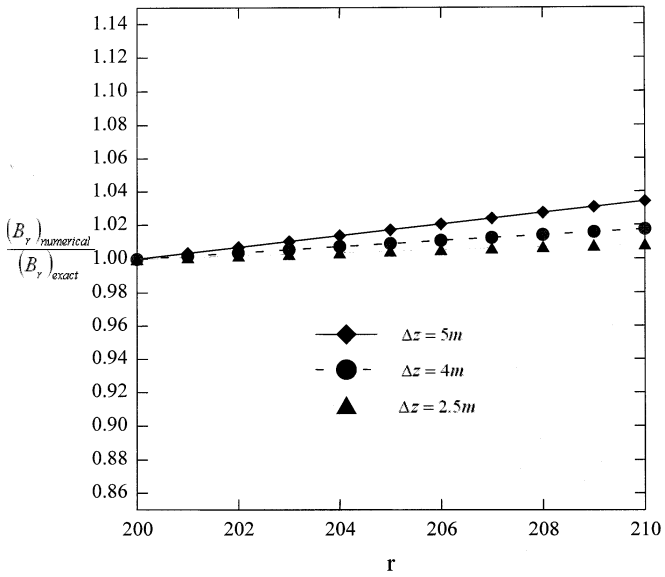

Fig. 4. The computed ratios between the numerical and exact solutions for the field variable B_r against r for the problem considered in Sec. 6.2.

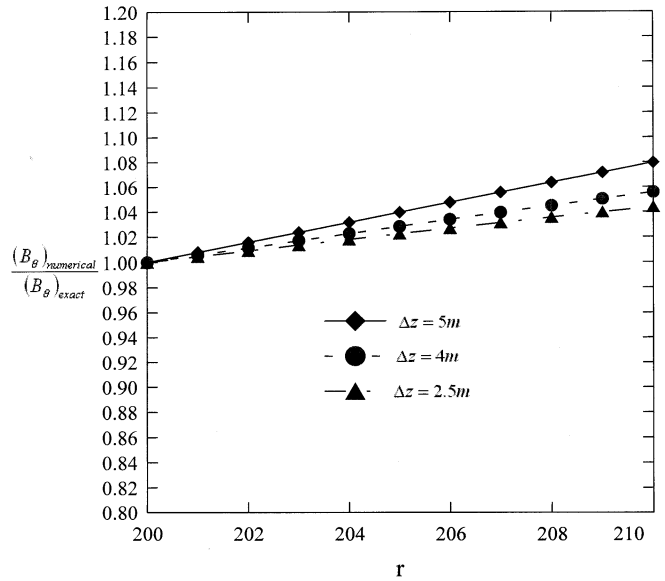

Fig. 5. The computed ratios between the numerical and exact solutions for the field variable B_θ against r for the problem considered in Sec. 6.2.

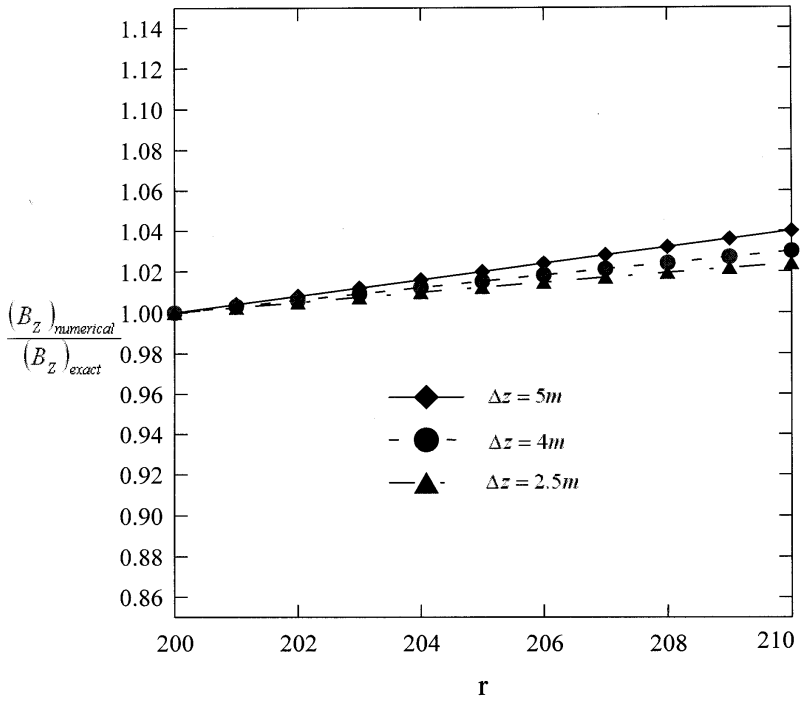

Fig. 6. The computed ratios between the numerical and exact solutions for the field variable B_z against r for the problem considered in Sec. 6.2.

Table 2. The computed L_2–*error* norms for A, B_r, B_θ, B_z, at different locations r for the test problem given in Sec. 6.2. These solutions are computed at different grid sizes, $\Delta = 4$ m and 5 m, from which the rates of convergence, $\log(err_1/err_2)/\log(\Delta z_1/\Delta z_2)$, are computed.

	A		
r	$\Delta = 5$ m	$\Delta = 4$ m	Rate
201	5.862480E−10	4.600200E−10	1.086620E+00
202	1.141590E−09	9.171250E−10	9.811330E−01
203	1.669270E−09	1.373780E−09	8.730720E−01
204	2.174080E−09	1.832210E−09	7.666930E−01
205	2.662100E−09	2.294220E−09	6.664880E−01
206	3.140360E−09	2.760990E−09	5.769740E−01
207	3.616320E−09	3.232980E−09	5.021550E−01
208	4.097370E−09	3.709890E−09	4.451980E−01
209	4.590250E−09	4.190560E−09	4.082580E−01
210	5.100580E−09	4.673060E−09	3.923040E−01

Table 2. (*Continued*)

B_r			
r	$\Delta = 5$ m	$\Delta = 4$ m	Rate
201	3.948080E−08	2.772370E−08	1.584300E+00
202	7.966860E−08	5.404860E−08	1.738750E+00
203	1.198260E−07	7.942560E−08	1.842850E+00
204	1.591010E−07	1.045540E−07	1.881460E+00
205	1.966180E−07	1.302190E−07	1.846550E+00
206	2.315650E−07	1.570910E−07	1.738950E+00
207	2.632670E−07	1.855460E−07	1.567900E+00
208	2.912380E−07	2.155640E−07	1.348380E+00
209	3.152150E−07	2.467200E−07	1.097950E+00
210	3.351650E−07	2.782460E−07	8.340700E−01
B_θ			
r	$\Delta = 5$ m	$\Delta = 4$ m	Rate
201	2.816990E−09	1.946550E−09	1.656380E+00
202	5.440910E−09	3.695900E−09	1.733060E+00
203	8.094050E−09	5.403780E−09	1.810630E+00
204	1.068260E−08	7.098820E−09	1.831500E+00
205	1.314160E−08	8.825800E−09	1.784070E+00
206	1.541670E−08	1.062220E−08	1.669350E+00
207	1.746500E−08	1.250630E−08	1.496640E+00
208	1.925750E−08	1.447130E−08	1.280490E+00
209	2.078060E−08	1.648570E−08	1.037570E+00
210	2.203570E−08	1.849780E−08	7.843020E−01
B_z			
r	$\Delta = 5$ m	$\Delta = 4$ m	Rate
201	4.342530E−10	2.945270E−10	1.739940E+00
202	8.713870E−10	5.846590E−10	1.788340E+00
203	1.304710E−09	8.753340E−10	1.788670E+00
204	1.726590E−09	1.172220E−09	1.735430E+00
205	2.129200E−09	1.480290E−09	1.629030E+00
206	2.505310E−09	1.802470E−09	1.475530E+00
207	2.848830E−09	2.138730E−09	1.284810E+00
208	3.155340E−09	2.485720E−09	1.068970E+00
209	3.422330E−09	2.837040E−09	8.405370E−01
210	3.649310E−09	3.183850E−09	6.114760E−01

6.3. *Analytic validation study in the fluid-elastic layer*

Having verified the code in both water and elastic layers, we can proceed to verify the code developed for modeling the fluid-elastic equations used together with the physically sound interface conditions. To the best of our knowledge, a closed-form solution to this coupled system of equations is still lacking. Therefore, we assign *a priori* an explicit source vector $\underline{f}_{9\times1}$ to (3.13) to make the resulting equation amenable to exact solutions given by

$$\phi(r,\, z,\, \theta) = r^2 z^6 \theta^3 + i r^2 z^6 \theta^3\,, \tag{6.11}$$

where ϕ stands for r, A^I, B_z^I, B_r^I, B_θ^I, A, B_z, B_r and B_θ.

As is usual in grid-independent tests, we carried out analyses on uniform grids of different resolutions. The solutions are computed on continuously refined grids and their prediction errors are cast in L_2–*error* norms. For completeness, we also plot field variables at $\theta = 5^\circ$ and $z = 50$ m against r. As shown in Figs. 7–11, the computed solutions were in good agreement when compared to the analytic data. This test validates the computer code developed on the personal computer ($Petuium\Pi$) to predict fluid-elastic wave propagation in three dimensions.

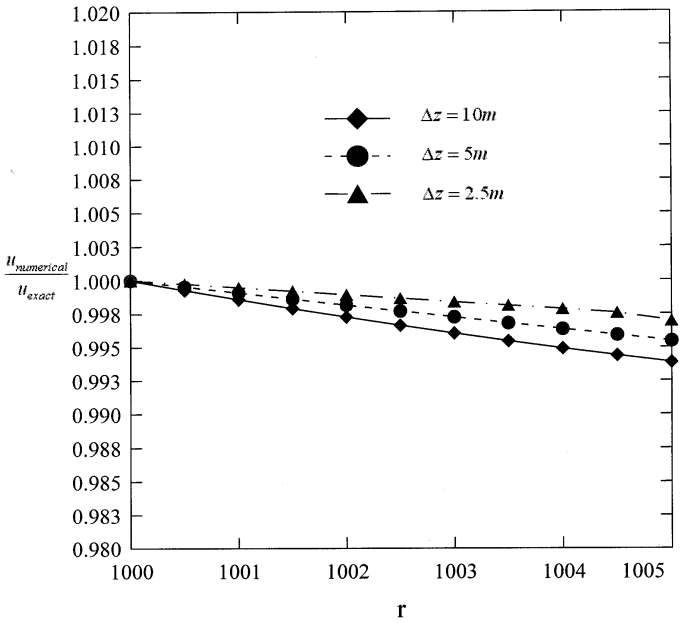

Fig. 7. The computed ratios between the numerical and exact solutions for the field variable u against r for the problem considered in Sec. 6.3.

7. Concluding Remarks

We have presented a finite difference scheme to solve a parabolized set of fluid-elastic equations. These three-dimensional equations are subject to physically relevant interface conditions. On the horizontal interface, we demand continuity of the normal displacement and

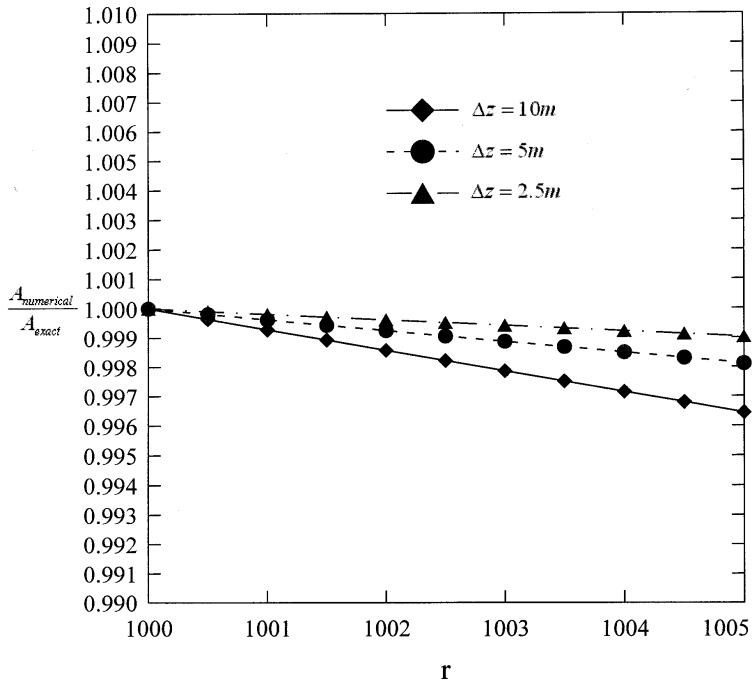

Fig. 8. The computed ratios between the numerical and exact solutions for the field variable A against r for the problem considered in Sec. 6.3.

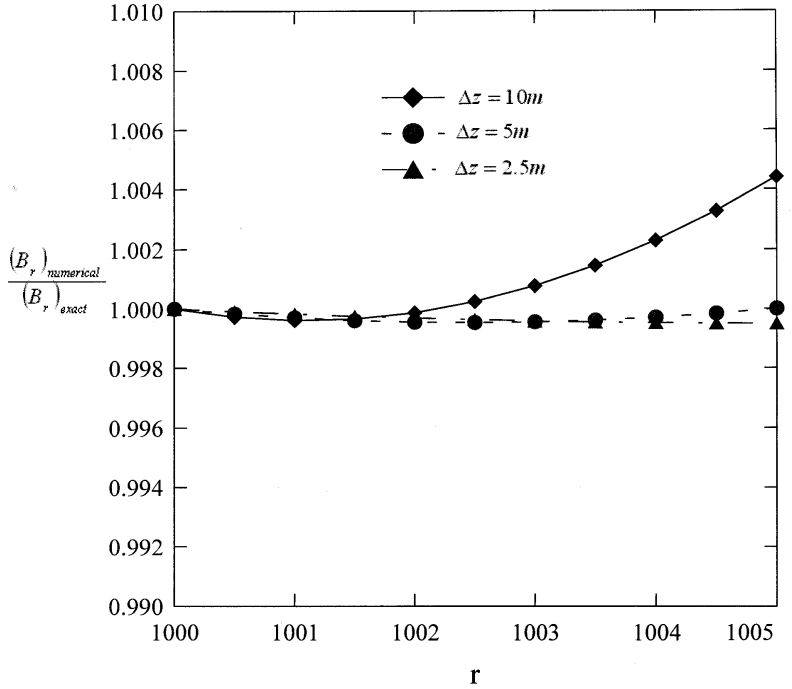

Fig. 9. The computed ratios between the numerical and exact solutions for the field variable B_r against r for the problem considered in Sec. 6.3.

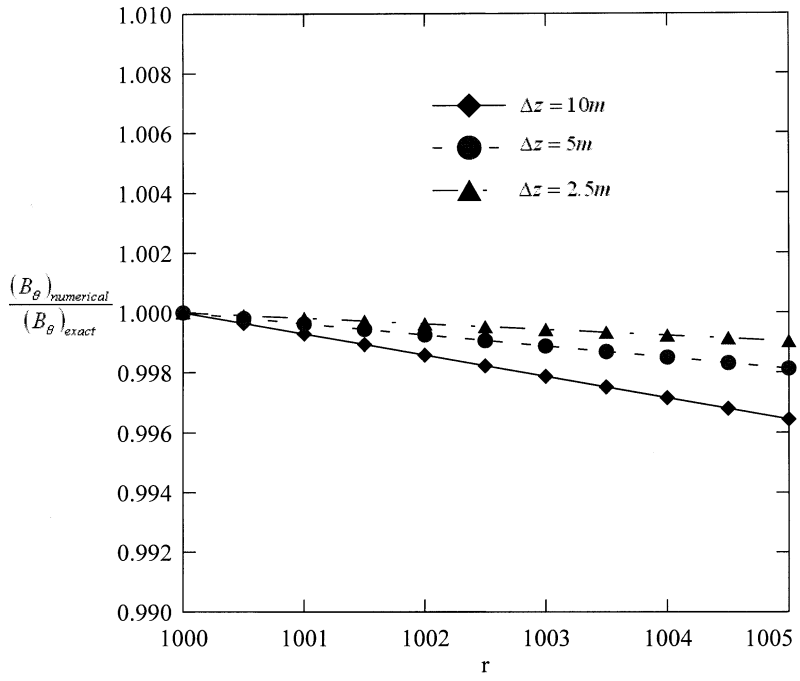

Fig. 10. The computed ratios between the numerical and exact solutions for the field variable B_θ against r for the problem considered in Sec. 6.3.

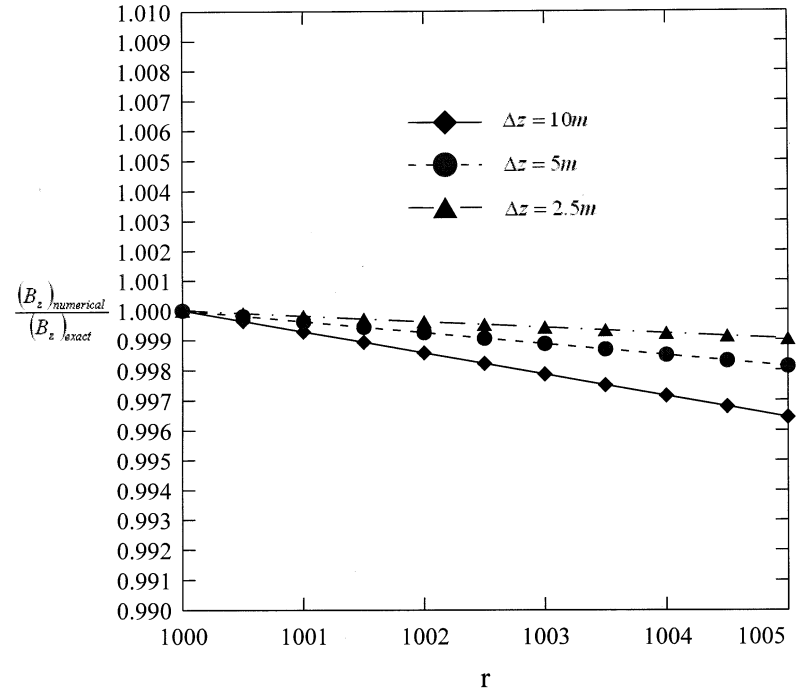

Fig. 11. The computed ratios between the numerical and exact solutions for the field variable B_z against r for the problem considered in Sec. 6.3.

the normal stress. In addition, physical reasoning requires that the shear stresses vanish on the interface for the present analysis which is formulated under the inviscid flow assumption. We discretize spatial derivatives with respect to θ and z using the second-order centered scheme. The resulting ordinary differential equation in r has been solved using the implicit Crank-Nicolson marching scheme to render second-order prediction accuracy in r. The proposed differential system formulated within the potential framework has been analytically verified. Three analytic test problems were chosen to demonstrate the applicability of the code to the individual fluid and elastic layer. We have also provided computational evidences to show that the code is applicable to analysis of wave propagation in water and elastic layers, in between which there is an interface.

Acknowledgments

The authors would like to express their sincere appreciation to the reviewers of the manuscript for providing important and helpful comments for the improvement of its content.

References

1. D. Lee and S. T. McDaniel, *Ocean Acoustic Propagation by Finite Difference Methods* (Pergamon Press, Oxford, 1988).
2. F. D. Tappert, "The parabolic equation approximation method," in *Wave Propagation and Underwater Acoustics*, Lecture Notes in Physics, Vol. 70, eds. J. B. Keller and J. S. Papadakis (Spring-Verlag, Heidelberg, 1977), pp. 224–284.
3. J. J. McCoy, "A parabolic theory of stress wave propagation through inhomogeneous linearly elastic solids," *J. Applied Mechanics*, **44** (1977), 462–468.
4. S. C. Wales and J. J. McCoy, "A comparison of parabolic wave theories for linearly elastic solids," *Wave Motion* **5** (1983), 99–113.
5. R. R. Greene, "A high-angle one-way wave equation for siesmic wave propagation along rough and sloping interfaces," *J. Acoust. Soc. Am.* **77** (1985), 1991–1998.
6. B. T. R. Wetton and G. Brooke, "One-way wave equations for seismoacoustic propagation in elastic waveguides," *J. Acoust. Soc. Am.* **87** (1990), 624–632.
7. D. J. Thomson and M. E. Mayfield, "An exact radiation condition for use with a posterior PE method," *J. Comp. Acoust.* **2**(2) (1994), 113–133.
8. J. S. Papadakis, "Exact, nonreflecting boundary conditions for the parabolic-type approximations in underwater acoustics," *J. Comp. Acoust.* **2**(2) (1994), 83–98.
9. M. D. Collins, "Higher-order and elastic parabolic equations for wave propagation in the ocean," in *Computational Acoustics: Seismo-Ocean Acoustics and Modeling*, eds. D. Lee, A. Cakmak and R. Vichnevetsky (North-Holland, Amsterdam, 1990), pp. 167–184.
10. M. D. Collins, "High-order, energy-conserving, two-way, and elastic parabolic equations," in *PE WORKSHOP II — Proc. 2nd Parabolic Equation Workshop*, eds. S. A. Chin-Bing, D. B. King, J. A. Davis and R. B. Evans, Naval Research Laboratory, Stennis Space Center (1993).
11. E. C. Shang and D. Lee, "A numerical treatment of the fluid/elastic interface under range-dependent environments," J. Acoust. Soc. Am. **85**(2) (1989), 654–660.
12. J. A. Hudson, "A parabolic approximation for elastic waves," *Wave Motion* **2** (1980), 207–214.
13. R. J. Nagem, D. Lee, and T. Chen, "Modeling elastic wave propagation in the ocean bottom," *J. Math. Model. Sci. Comput.* **2**(4) (1995), 1–10.
14. D. Lee and R. J. Nagem, "An interface model for coupled fluid-elastic parabolic equations,"

Proc. 3rd European Conf. Underwater Acoust., Vol. 1, ed. J. S. Papadakis, FORTH-IACM, Heraklion (1996), pp. 159–164.
15. D. Lee, R. J. Nagem, D. C. Resasco, and C. F. Chen, "A coupled 3D fluid-elastic wave propagation model: Mathematical formulation and analysis," *Applicable Analysis* **68** (1998), 147–178.
16. D. Lee and M. H. Schultz, *Numerical Ocean Acoustic Propagation in Three Dimensions* (World Scientific, Singapore, 1995).
17. J. D. Achenbach, *Wave Propagation in Elastic Solids* (North-Holland, 1987).
18. S. C. Chen, "On a mathematical formulation of ocean acoustics in an environment including elastic bottom," Master Thesis, Department of Naval Architecture and Ocean Engineering, National Taiwan University, May 1998.
19. J. Crank and P. Nicolson, "A practical method for numerical evaluation of solutions of partial differential equations of the heat-conduction type," *Proc. Cambridge Philos. Soc.*, Vol. 43 (1947), pp. 50–67.
20. R. D. Richtmyer and K. W. Morton, *Difference Methods for Initial-Value Problems*, 2nd ed. (Interscience Publishers, Wiley, New York, 1967).
21. J. C. Tannehill, D. A. Anderson, and R. H. Pletcher, *Computational Fluid Mechanics and Heat Transfer*, 2nd ed. (Taylor & Francis, London, 1997).
22. W. M. Ewing, W. S. Jarditzky, and F. Press, *Elastic Waves in Layered Media* (McGraw-Hill, New York, 1957).
23. Rayleigh, *Theory of Sound*, Vol. II (Dover Publications, 1945), pp. 424–427.
24. D. Lee, R. J. Nagem and D. C. Resasco, "Numerical computation of elastic wave equations," *J. Comput. Acoust.* **5**(2) (1997), 157–176.